Available online at www.sciencedirect.com

ScienceDirect

Ceramics International 40 (2014) 2427–2434

CERAMICS INTERNATIONAL

www.elsevier.com/locate/ceramint

XRD and Raman study on crystal structures and dielectric properties of $Ba[Mg_{(1-x)/3}Zr_xNb_{2(1-x)/3}]O_3$ solid solutions

Han Zhang[a], Chuanling Diao[a,1], Shulian Liu[b,1], Shouzhen Jiang[a,*], Xiping Jing[c], Feng Shi[a,*]

[a]College of Physics and Electronics, Shandong Normal University, Jinan 250014, PR China
[b]Shandong Cadre School of Quality and Technical Supervision, Jinan 250014, PR China
[c]Beijing National Laboratory for Molecular Sciences, State Key Laboratory of Rare Earth Materials Chemistry and Applications, College of Chemistry and Molecular Engineering, Peking University, Beijing 100871, PR China

Received 20 June 2013; received in revised form 4 August 2013; accepted 4 August 2013
Available online 11 August 2013

Abstract

$Ba[Mg_{(1-x)/3}Zr_xNb_{2(1-x)/3}]O_3$ (BMZN, $x=0$, 0.05, 0.1, 0.15) solid solution ceramics were synthesized via conventional solid-state reactions. Crystal structures were studied using X-ray diffraction, and vibrational modes were investigated using Raman spectroscopy. Crystal symmetry increased with increasing Zr^{4+} content, with a transformation from a hexagonal to a cubic structure observed. For BMZN ceramics, oxygen octahedron distortion occurred where $x=0.05$, and the ordered phase changed from 1:2 to 1:1. The dielectric constant had a positive correlation with the full width at half maximum (FWHM) of the A_{1g}(O) phonon mode, and the Raman shift of the A_{1g}(Nb) mode. The dielectric constant had an inverse correlation with the Raman shift of the A_{1g}(O) phonon mode. The temperature coefficient of capacitance had an inverse correlation with the Raman shift of the A_{1g}(Nb) mode, and the dielectric loss had an inverse correlation with the FWHM of the A_{1g}(Nb) mode.

Keywords: C. Dielectric properties; Microwave dielectric ceramics; Raman spectra; Crystal structures; Vibrational modes

1. Introduction

$Ba(B'_{1/3}B''_{2/3})O_3$-type microwave dielectric ceramics (B′=Mg, Zn, Ni and Co; B″=Ta and Nb) have promising applications as components in resonators and filters [1–4]. $Ba(Mg_{1/3}Nb_{2/3})O_3$ (BMN) ceramic in particular is promising in microwave communication systems. This is because of its favorable dielectric properties including dielectric constant $\varepsilon_r=25.4$, quality factor $Q=5600$ at 10.5 GHz, and temperature coefficient of capacitance $\tau_c \approx -24\times10^{-6}/°C$ [5,6].

The sequencing of B-site cations in microwave dielectric materials is an important factor affecting the structure and dielectric properties of complex perovskite microwave dielectric ceramics [7–11]. Substitution at the B-site can modulate the structure and properties of solid solutions [12–17]. BMN has a hexagonal ($P\bar{3}m1$) 1:2 ordered structure, and $BaZrO_3$ (BZ) ceramic has a cubic ($Pm3m$) structure with a lattice constant of $a=0.4180$ nm. The average ionic radius of $Mg_{1/3}Nb_{2/3}$ at the B-site is 0.667 Å, whereas that of Zr^{4+} is ~0.72 Å [18,19]. The complete solid solution of these ions can be synthesized by substituting Mg^{2+} and Nb^{5+} at the B-site by Zr^{4+}, to form $Ba[Mg_{(1-x)/3}Zr_xNb_{2(1-x)/3}]O_3$ (BMZN, $x=0$, 0.05, 0.1, 0.15), because the difference between their ionic radii is $<15\%$.

The ordered structures and dielectric properties of BMN ceramics have been extensively investigated, with a major focus on their crystal structures and phase transition using X-ray diffraction (XRD) [17,19]. Studies on B-site substitution of tetravalent ions and the effect on crystal structure, phase transition, and vibrational modes are limited. Raman spectroscopy is very sensitive to crystal structure variation, and is useful for investigating phonon modes and crystal structures of solid solutions [2,11,20–25].

In the current study, the crystal structures, phase transitions, and dielectric properties of BMZN ceramics are analyzed using

*Corresponding authors. Tel./fax: +86 531 86182521.
E-mail addresses: jiang_sz@126.com (S. Jiang), sf751106@sina.com.cn (F. Shi).
[1]Joint first author.

0272-8842/$ - see front matter © 2013 Elsevier Ltd and Techna Group S.r.l. All rights reserved.
http://dx.doi.org/10.1016/j.ceramint.2013.08.016

XRD and Raman spectroscopy. The relationship between crystal structure and dielectric properties is investigated using lattice vibrational modes as the medium. This study aims to provide a reference for correlating lattice vibrational modes, crystal structures, and dielectric properties of $Ba(B'_{1/3}B''_{2/3})O_3$ type solid solutions.

2. Experimental

Raw materials were analytically pure $BaCO_3$, ZrO_2, $4MgCO_3 \cdot Mg(OH)_2 \cdot 5H_2O$, and Nb_2O_5 powders. BMZN solid solutions were synthesized via a conventional solid-state sintering technique. Oxide compounds were mixed for 12 h in polyethylene jars with zirconia balls, then dried and calcined at 1200 °C for 2 h. After re-milling, the powders were dried and pressed into 15×1 mm^2 discs and sintered at 1520 °C for 3 h.

A Hewlett Packard 4278A capacitance meter was used to test the capacitance (C) and dielectric loss ($\tan\delta = 1/Q$) at 1 MHz. The dielectric constant (ε_r) was calculated using the equation $\varepsilon_r = 14.4 \times C \times d/D^2$, where D and d are the average diameter and thickness of the sample, respectively. The temperature coefficient of the capacitance (τ_c) was calculated using the equation $\tau_c = (C_{85} - C_{25})/(60 \times C_{25})$, where C_{85} and C_{25} are the capacitances of the sample at 85 °C and 25 °C, respectively.

XRD analyses were carried out using a Rigaku D/max-rB X-ray diffractometer, with a Cu-K_α incident source in the 10^{-1} 20° 2θ range. Raman scattering spectra were obtained at room temperature using a Nexus 670 spectrometer, equipped with a liquid N_2-cooled CCD detector and an Olympus BXL microscope ($100\times$ and $20\times$ objectives). Measurements were recorded in backscattering geometry using a Nd:YVO_4 laser, with the 514-nm line as the excitation source (0.103 W). Accumulation times were typically 10 collections every 5 s, and the spectral resolution was better than 2 cm^{-1}.

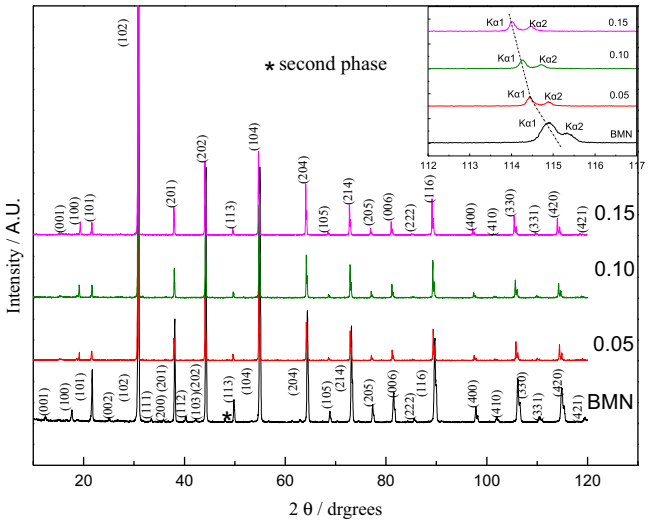

Fig. 1. XRD patterns of BMZN solid solutions after sintering at 1520 °C for 3 h.

3. Results and discussion

XRD patterns of BMZN with differing x are shown in Fig. 1. The main crystalline phase is that of the BMZN solid solution, which is indexed to JCPDS card nos. 17-0173 and 06-0399. When $x \geq 0.05$, the solid solution is phase pure. However, when $x = 0$, a second phase of $Ba_5Nb_4O_{15}$ (JCPDS card no. 14-0028) emerges in the BMN ceramic. The (420) diffraction peak at a high angle shifts to a lower angle with increasing Zr^{4+} content, and the cell constant of the BMZN solid solution increases. The splitting of the (420) diffraction peak indicates distortion of the O octahedron [26,27]. Importantly, the crystal structure converts from a hexagonal to a cubic structure with increasing Zr^{4+} content.

Ordered structures [26–28] are observed at low angle in the XRD pattern of the BMZN solid solution, as shown in Fig. 2. Diffraction peaks of the 1:2 ordered structure emerge at $2\theta \approx 17.7$, 38.1, and 40.7°. Conversion between the two ordered phases in the BMZN solid solution occurs with increasing Zr^{4+} content. The 1:2 ordered structure where $x = 0$, coexistence of 1:2 and 1:1 ordered structures where $x = 0.05$, and 1:1 ordered structure where $x = 0.10$ and 0.15 are

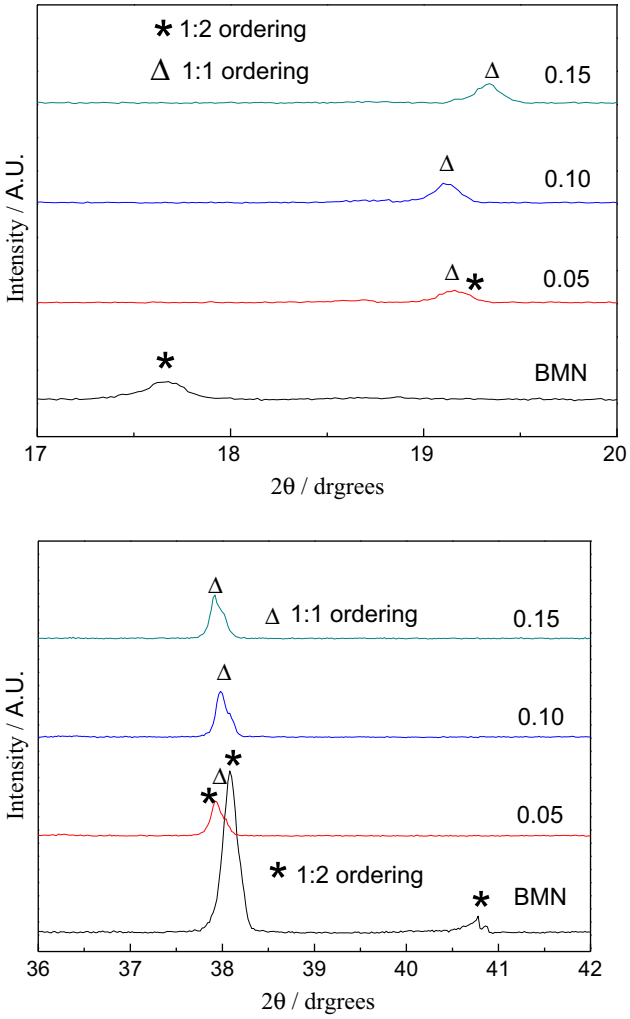

Fig. 2. XRD patterns showing changes in the ordered structure at a low angle.

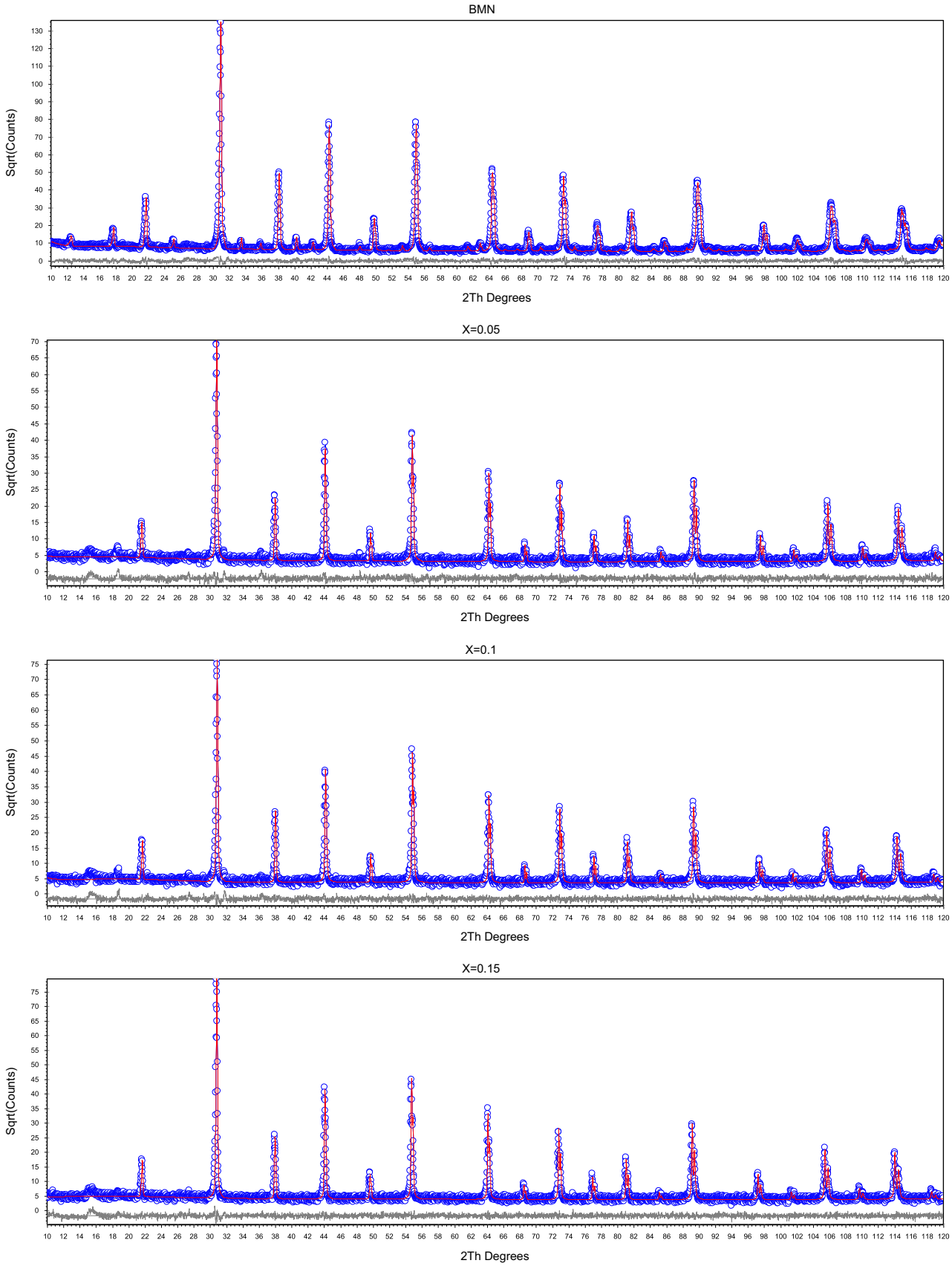

Fig. 3. Refined XRD patterns.

observed, in agreement with results of Akbas et al. [19]. The conversion between the two ordered phases is caused by the replacement of Mg^{2+} and Nb^{5+} by Zr^{4+}. Zr^{4+} randomly occupies B′- and B”-sites. The coulombic repulsion between the cations decreases, and the displacement of O^{2-} regulates the B′–O and B′′–O bond length difference. This results in a stable 1:1 ordered structure [28]. The degree of distortion about the O octahedron is weakened with increasing Zr^{4+} content, which results in the conversion of the ordered phase from 1:2 to 1:1 and the decrease in ordering degree. The increase in structural symmetry is closely related to the decrease in O octahedron distortion. Correspondingly, the ordering degree decreases with increasing Zr^{4+} content.

Refined XRD patterns of BMZN solid solutions are shown in Fig. 3. They show that the crystal structure converts from hexagonal to cubic with increasing Zr^{4+} content, similarly to results in Fig. 1.

Table 1 shows refined XRD parameters and lattice constants of BMZN ceramics. Lattice constants increase with increasing Zr^{4+} content. When $x=0$, BMN has a hexagonal structure and cell volume of 204.798 Å^3. Cell volumes of BMZN solid solutions with increasing Zr^{4+} content are 68.7, 69.0 and 69.4 Å^3. When $x=0.05$, the crystal structure transforms to cubic, and the cell volume significantly decreases. When $x>0.05$, BMZN exhibits a cubic structure, the ionic radius increases, and the cell volume gradually increases.

The ε_r increases with increasing Zr^{4+} content, whereas τ_c decreases. According to the logarithmic mixing law, the relative ε_r in the mixed system is related to that of the constituent phases by the following formula:

$$\ln\varepsilon_r = X_1\ln\varepsilon_{r1} + X_2\ln\varepsilon_{r2} + \ldots + X_n\ln\varepsilon_{rn}; X_1 + X_2 + \ldots X_n = 1$$

X_1, X_2, …, X_n represent the volume fractions of the constituent phases in the mixed system. ε_r, ε_{r2}, …, ε_{rn} represent the relative dielectric constants of the constituent phases. The ε_r of BZ (40) is larger than that of BMN (25.4) [20], therefore the ε_r of BMZN increases with increasing Zr^{4+} content. Similarly, τ_c of the BZ ceramic ($\approx -310\times10^{-6}$/°C) is less than that of BMN ($\approx -24\times10^{-6}$/°C) [19], indicating a negative shift of τ_c in the BMZN system with increasing Zr^{4+} content.

The Raman spectrum of the system is shown in Fig. 4. Seven Raman modes [20,23] are identified in the spectrum of phase pure BMN. Each Raman mode of the BMZN solid solution exhibits significant position and intensity changes with increasing Zr^{4+} content. Changes in the Raman frequency and full width at half maximum (FWHM) are caused by changing Zr^{4+} content, and are two important parameters for identifying normal Raman modes. The wavenumber and FWHM values of phonon modes are shown in Table 2.

Table 1
Refined XRD parameters and lattice constants of BMZN ceramics.

	BMN	0.05	0.1	0.15
a (Å)	5.7788	4.096	4.1019	4.1084
b (Å)	5.7788	4.096	4.1019	4.1084
c (Å)	7.081	4.096	4.1019	4.1084
R_P (%)	7.33	12.73	11.52	11.8
R_{WP} (%)	10.99	19.894	17.96	17.35
ε_r	25.4	33.9	35.8	37.2
τ_c^*	−24	−60.93	−101.8	−103.2
tan $\delta^{\star}$	1.13	1.2	1.89	1.88

$^{\star}\times10^{-4}$, * $\times10^{-6}$/°C, Weighted profile *R*-factor: R_{WP}, [29], Profile *R*-factor: R_P [29].

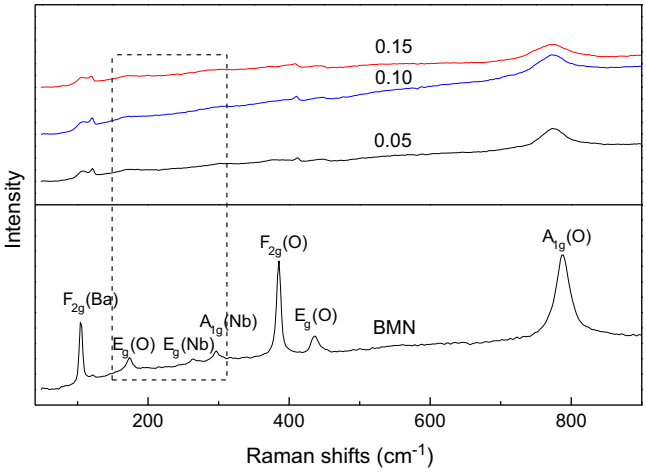

Fig. 4. Raman spectrum at Raman shift from 100 to 900 cm^{-1}.

Table 2
Phonon mode wavenumber and FWHM parameters.

	BMN		0.05		0.1		0.15	
	Wavenumber (cm^{-1})	FWHM	Wavenumber (cm^{-1})	FWHM	Wavenumber (cm^{-1})	FWHM	Wavenumber (cm^{-1})	FWHM
F_{2g}(Ba)	104	4.4	108	12.6	108	3.8	107	5.6
		–	121	3.2	120	4.02	119	3.8
E_g(O)	173	8.2	177	6	172	8.3	172	12.8
E_g(Nb)	263	8.3	–	–	–	–	–	–
A_{1g}(Nb)	296	9	302	4.6	304	3.6	306	4.5
F_{2g}(O)	385	6.9	380	40.3	410	6.6	403	29
E_g(O)	436	12.8	447	29	445	16	437	32
A_{1g}(O)	788	23	775	37	774	45	773	59

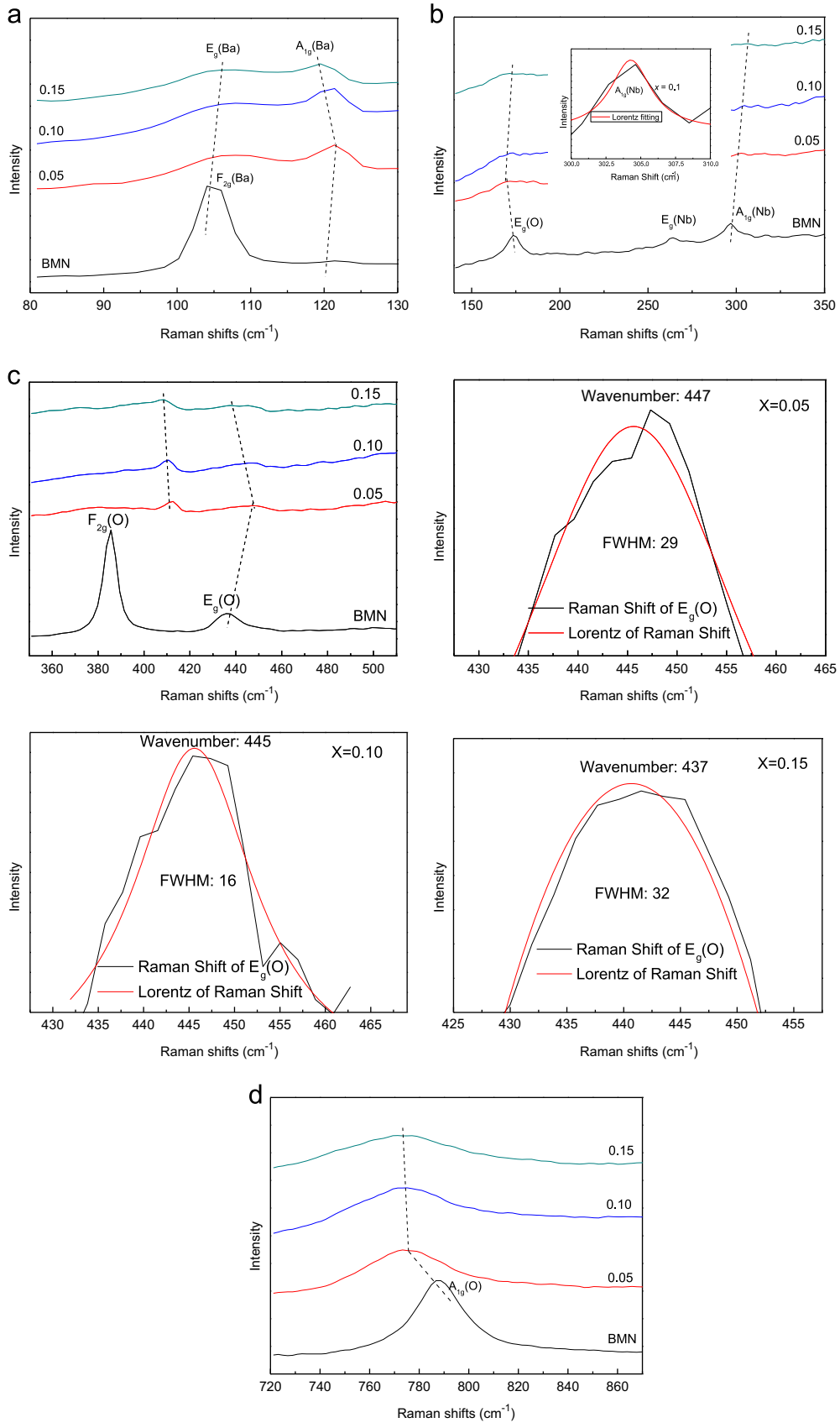

Fig. 5. Raman spectra of BMZN solid solutions. (a) Phonon mode related to Ba^{2+} near 105 cm^{-1}, (b) phonon mode at 150–350 cm^{-1} and (c) phonon mode related to O^{2+} at 350–450 cm^{-1}. (c1) Lorentz fitting of Eg(O) when x is (c1) 0.05, (c2) 0.10, and (c3) 0.15. (d) Stretching mode of the O octahedron near 788 cm^{-1}.

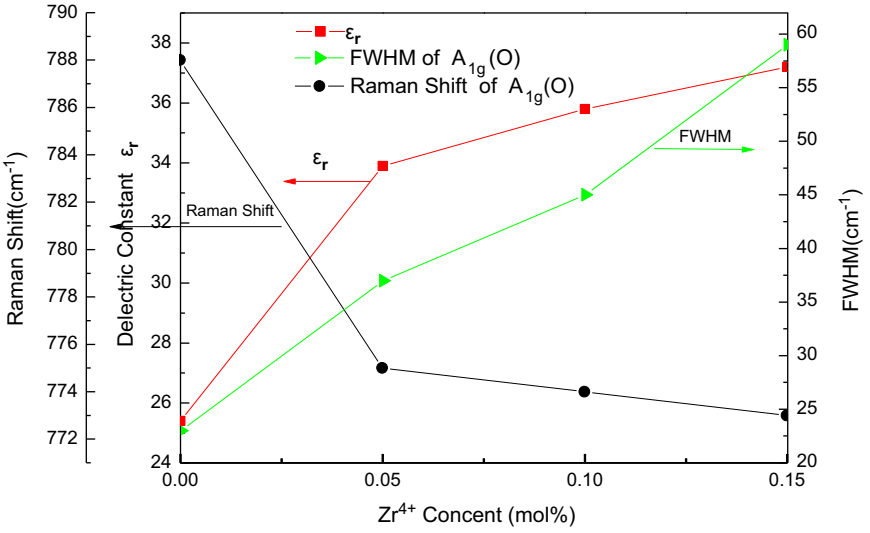

Fig. 6. Correlation between dielectric constant of the A_{1g}(O) phonon mode, FWHM, and Raman shift, with increasing Zr^{4+} content.

According to Fig. 5 and Table 2, the intensities of Raman peaks decrease with increasing Zr^{4+} content. When $x \geq 0.05$, the E_g(Nb) mode disappears, and the intensity of the A_{1g}(Nb) mode decreases. This is because of the decreasing Nb^{5+} content at the B′′-site, and the increasing Zr^{4+} content. Siny et al. [20] proposed that samples with high ordering degrees exhibit strong Raman peaks. Raman active modes are closely related to the structure order. Fig. 4 shows that the intensities of Raman peaks of BMN are stronger than those of BMZN, because its ordering degree is higher than that of BMZN with additional Zr^{4+} (as determined by XRD analysis). The intensities of A_{1g}(O) diffraction peaks also decrease with increasing Zr^{4+} content. The change in the Raman spectrum also indicates that the crystal structure of the BMZN solid solution is transformed with increasing Zr^{4+} content, which is consistent the XRD analysis.

The lowest frequency modes ($F_{2g}=A_{1g}+E_g$) of the BMZN solid solution near 106 cm^{-1} are generated by the lattice vibration related to Ba^{2+}. As shown in Fig. 5a, F_{2g}(Ba) splits into E_g(Ba) and A_{1g}(Ba), with E_g(Ba) shifting to a higher angle, and A_{1g}(Ba) to a lower angle. As shown in Fig. 5b, the A_{1g}(Nb) mode shifts to a higher wavenumber with increasing Zr^{4+} content. The FWHM of the A_{1g}(Nb) mode decreases with increasing Zr^{4+} content, because the radii of B-sites increases upon replacing Mg^{2+} and Nb^{5+} with Zr^{4+}. Shifts of the F_{2g}(O), E_g(O) and A_{1g}(O) modes occur when $x=0.05$, with the F_{2g}(O) and E_g(O) modes shifting to a higher angle and the A_{1g}(O) mode to a lower angle (Fig. 5c).

FWHM values and wavenumber data of Eg(O) modes were obtained from the Lorentz fitting, as shown in Fig. 5c(1), c(2), and c(3). A_{1g}(O) stretching modes of the O octahedron are shown in Fig. 5d, where values are in the range 773–788 cm^{-1}. A_{1g}(O) is the highest intensity vibrational mode, and is related to the O octahedron vibration of the ordered phase [24,25]. The FWHM of the A_{1g}(O) phonon mode gradually increases with increasing Zr^{4+} content, and the Raman shift decreases. Both phenomena are related to the decreasing ordered phases with increasing Zr^{4+} substitution. When $x \geq 0.05$, the degree of the 1:1 ordered structure gradually increases.

The relationship between the FWHM of A_{1g}(O) phonon mode, Raman shift, and ε_r is shown in Fig. 6. FWHM gradually increases, Raman shift decreases, and ε_r increases with increasing Zr^{4+} content. The changes in ε_r and Raman shift occur when $x=0.05$. A significant structural change of the BMZN solid solution also occurs at $x=0.05$, in agreement with the XRD results. That is, the BZMN crystal structure changes from a 1:2 to 1:1 ordered structure, with increasing Zr^{4+} content. Therefore, the ε_r has a positive correlation with the FWHM of the A_{1g}(O) phonon mode, and an inverse correlation with its Raman shift. The increase in ε_r is caused by the increasing Zr^{4+} content, which is proved by the logarithmic mixing law. The FWHM of the A_{1g}(O) mode also increases, because of the decrease in O octahedron distortion. Thus, a positive correlation exists between these two values. The Raman shift decreases because of the decrease in ordering degree with increasing Zr^{4+} content, so an inverse correlation exists between the ε_r and Raman shift of the A_{1g}(O) mode.

The relationship between the Raman shift of A_{1g}(Nb), ε_r, and τ_c is shown in Fig. 7. The Raman shift of A_{1g}(Nb) and ε_r gradually increases with increasing Zr^{4+} content, whereas τ_c decreases. When $x=0.05$, the Raman shift and ε_r of A_{1g}(Nb) undergo significant changes compared with those of BMN, confirming that significant structural change of BMN occurs after Zr^{4+} is added (i.e., the distortion of O octahedra caused by Zr^{4+} substitution). The Raman shifts of the A_{1g}(Nb) mode has a positive correlation with ε_r and an inverse correlation with τ_c. As shown in Fig. 5b, the A_{1g}(Nb) mode shifts to higher wavenumber with increasing Zr^{4+} substitution. This is related to the decrease in ordering degree, caused by the increase in radii of B-site ions, and ε_r also increases. The interaction between Zr^{4+} and O^{2-} can strengthen the external

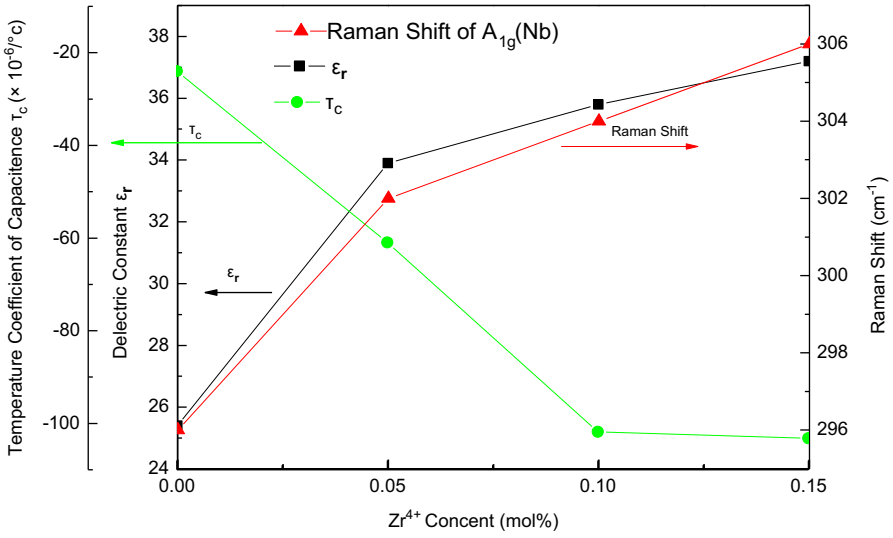

Fig. 7. Correlation between Raman shift of A_{1g}(Nb), dielectric constant, and volumetric temperature coefficient, with increasing Zr^{4+} content.

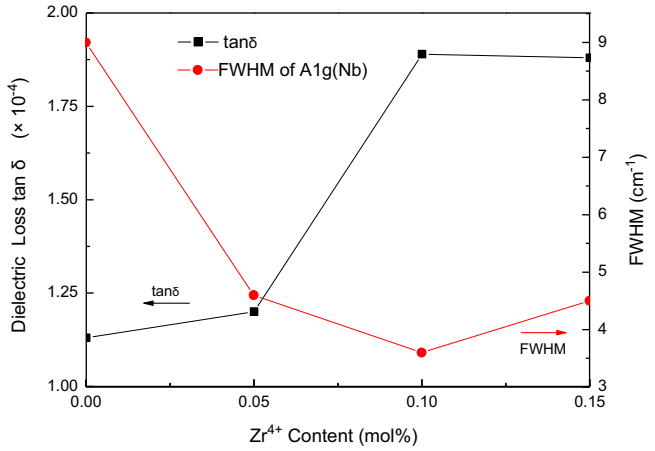

Fig. 8. Correlation between FWHM of the A_{1g}(Nb) phonon mode and dielectric loss, with increasing Zr^{4+} content.

electric field, being more powerful than the interaction between other homogeneous B-site ions (such as Nb^{5+}) and O^{2-}. This results in a strong internal electric field. The polarization between Zr^{4+} and O^{2-} is strengthened, and the dipole moment of the polar molecule increases, causing a large ε_r. With substitution by Zr^{4+} for B-site ions, a tiny deviation occurs in the relative equilibrium position between the positive and negative ions. That is, the O octahedron distortion is weakened with increasing Zr^{4+} content, resulting in the A_{1g}(Nb) mode shifting to a higher angle. In summary, the positive correlation between ε_r and A_{1g}(Nb) mode shift is caused by increasing Zr^{4+} content.

The contribution of different types of polarization on τ_c is different, because ions with large deformation have larger electronic polarization rates. With the substitution by Zr^{4+} for B-site ions, the deformation of B-site ions become larger, and the electronic polarization rate increases. This can result in negative τ_c. Therefore, the decrease in τ_c is also caused by increasing Zr^{4+} content, i.e., the increase in electronic polarization rate. An inverse correlation exists between the A_{1g}(Nb) mode shift and τ_c.

The relationship between the FWHM of the A_{1g}(Nb) mode and the dielectric loss is shown in Fig. 8. Dielectric loss increases with increasing Zr^{4+} content, while FWHM decreases. An inverse correlation exists between the FWHM and dielectric loss. This shows that the dielectric loss is closely related to the FWHM, which is consistent with results of Webb et al. [23]. The ordering degree decreases with the increase in the radii of B-site ions, which results in the increased dielectric loss [30]. As shown in Fig. 5b, the FWHM of A_{1g}(Nb) decreases with increasing Zr^{4+} content, which is related to the decrease in ordering degree of B-site ions. An inverse correlation exists between the FWHM and dielectric loss.

4. Conclusions

The crystal structures and dielectric properties of BMZN microwave dielectric ceramics synthesized via solid-state reaction were characterized by XRD and Raman spectroscopy. The relationship between Raman modes, crystal structure, and dielectric properties was investigated. Adding $BaZrO_3$ had a significant effect on the crystal structure and dielectric properties of BMZN. The symmetry of the BMZN solid solution was improved, and its crystal structure converted from hexagonal to cubic, with increasing Zr^{4+} content. The lattice constant decreased accordingly, and the ordered phases gradually transformed from a 1:2 to 1:1 structure. The dielectric constant has a positive correlation with the FWHM of the A_{1g}(O) phonon mode and Raman shift of the A_{1g}(Nb) mode. The dielectric constant has an inverse correlation with the Raman shift of the A_{1g}(O) phonon mode. The temperature coefficient of capacitance had an inverse correlation with the Raman shift of the A_{1g}(Nb) mode, and the dielectric loss has an inverse correlation with the FWHM of the A_{1g}(Nb) mode.

Acknowledgments

We are grateful for financial support from the National Nature Science Foundation of China (No. 21071009).

References

[1] T.A. Vanderah, Talking ceramics, Science 298 (2002) 1182–1184.
[2] F. Shi, H.L. Dong, Correlation of phonon characteristics and crystal structural of $Ba[Zn_{1/3}(Nb_{1-x}Ta_x)_{2/3}]O_3$ solid solutions, Journal of Applied Physics 111 (2012) 014–111.
[3] H. Hughes, D.M. Iddles, I.M. Reaney, Niobate-based microwave dielectrics suitable for third generation mobile phone base stations, Applied Physics Letters 79 (2001) 2952–2954.
[4] J.I. Yang, S. Nahm, C.H. Choi, H.J. Lee, H.M. Park, Microstructure and microwave dielectric properties of $Ba(Zn_{1/3}Ta_{2/3})O_3$ ceramics with ZrO_2 addition, Journal of the American Ceramic Society 85 (2002) 165–168.
[5] M.W. Lufaso, Crystal structures, modeling, and dielectric property relationships of 2:1 Ordered $Ba_3MM'_2O_9$ (M=Mg, Ni, Zn; M′= Nb, Ta) perovskites, Chemistry of Materials 16 (2004) 2148–2156.
[6] A. Dias, R.L. Moreira, Far-infrared spectroscopy in ordered and disordered $Ba(Mg_{1/3}Nb_{2/3})$ O_3 microwave ceramics, Journal of Applied Physics 94 (2003) 3414–3421.
[7] P.K. Davies, J. Tong, T. Negas, Effect of ordering-induced domain boundaries on low-loss $Ba(Zn_{1/3}Ta_{2/3})O_3$–$BaZrO_3$ perovskite microwave dielectrics, Journal of the American Ceramic Society 80 (1997) 1727–1740.
[8] G. Rong, N. Newman, B. Shaw, D. Cronin, Role of Ni and Zr doping on the electrical, optical, magnetic, and structural properties of barium zinc tantalate ceramics, Journal of Materials Research 14 (1999) 4011–4019.
[9] H. Matsumoto, H. Tamura, K. Wakino, Ba(Mg, Ta)O_3–$BaSnO_3$ high-Q dielectric resonator, Japanese Journal of Applied Physics 30 (1991) 2347–2349.
[10] Z.X. Xiong, Research Methodology of Inorganic Materials, Xiamen University Press, Xiamen, 2001 (in Chinese).
[11] B.K. Kim, H. Hamaguchi, I.T. Kim, et al., Probing of 1:2 ordering in $Ba(Ni_{1/3}Nb_{2/3})O_3$ and $Ba(Zn_{1/3}Nb_{2/3})O_3$ ceramics by XRD and raman spectroscopy, Journal of the American Ceramic Society 78 (11) (1995) 3117–3120.
[12] S. Kawashima, M. Nishida, I. Ueda, H. Ouchi, $Ba(Zn_{1/3}Ta_{2/3})O_3$ Ceramics with low dielectric loss at microwave frequencies, Journal of the American Ceramic Society 66 (1983) 421–423.
[13] K. Endo, K. Fujimoto, K. Murakawa, Dielectric properties of ceramics in $Ba(Co_{1/3}Nb_{2/3})O_3$–$Ba(Zn_{1/3}Nb_{2/3})O_3$ solid solution, Journal of the American Ceramic Society 70 (1987) 215–218.
[14] S.B. Desu, H.M. O'Bryan, Microwave loss quality of $Ba(Zn_{1/3}Ta_{2/3})O_3$ Ceramics, Journal of the American Ceramic Society 68 (1985) 546–551.
[15] H. Tamura, T. Konoike, Y. Sakabe, K. Wakino, Improved high Q dielectric resonator with complex perovskite structure, Journal of the American Ceramic Society 67 (1984) C59–C61.
[16] F. Galasso, J. Pyle, Preparation and study of ordering in $A(B'_{0.33}$ $Nb_{0.67})$ O_3 perovskite -type compounds, Journal of Physical Chemistry 67 (1963) 1561–1562.
[17] C.T. Lee, Y.C. Lin, C.Y. Huang, Cation ordering and dielectric characteristics in barium zinc niobate, Journal of the American Ceramic Society 90 (2007) 483–489.
[18] R.D. Shannon, Revised effective ionic radii and systematic studies of interatomic distances in halides and chalcogenides, Acta Crystallographica A32 (1976) 751–767.
[19] M.A. Akbas, P.K. Davies, Ordering-induced microstructures and microwave dielectric properties of the $Ba(Mg_{1/3}Nb_{2/3})O_3$–$BaZrO_3$ system, Journal of the American Ceramic Society 81 (3) (1998) 670–676.
[20] I.G. Siny, R. Tao, R.S. Katiyar, et al., Raman spectroscopy of Mg–Ta order–disorder in $Ba(Mg_{1/3}Ta_{2/3})O_3$, Journal of Physics and Chemistry of Solids 59 (1998) 181–195.
[21] F. Shi, H.L. Dong, Vibrational modes and structural characteristics of $(Ba_{0.3}Sr_{0.7})[(Zn_xMg_{1-x})_{1/3}Nb_{2/3}]O_3$ solid solutions, Dalton Trans. 40 (2011) 11591–11598.
[22] H.L. Dong, F. Shi, Vibration spectra and structural characteristics of Ba $[(Zn_{1-x}Mg_x)_{1/3}Nb_{2/3}]$ O_3 Solid Solutions, Applied Spectroscopy Reviews 46 (2011) 207–221.
[23] S.J. Webb, J. Breeze, R.I. Scott, D.S. Cannell, D.M. Iddles, N.M. Alford, Raman spectroscopic study of gallium-doped $Ba(Zn_{1/3}Ta_{2/3})O_3$, Journal of the American Ceramic Society 85 (2002) 1753–1756.
[24] C.T. Cha, Y.C. Chen, H.F. Cheng, et al., Correlation of microwave properties and normal vibration modes of xBa$(Mg_{1/3}Ta_{2/3})O_3$–(1–x)Ba $(Mg_{1/3}Nb_{2/3})O_3$ ceramics, Journal of Applied Physics 94 (2003) 3360–3364.
[25] T. Nagai, M. Sugaiyama, M. Sando, et al., Anomaly in the infrared active phonon modes and its relationship to the dielectric constant of $(Ba_{1-x}Sr_x)$ $(Mg_{1/3}Ta_{2/3})O_3$ compound, Journal of Applied Physics 35 (1996) 5163–5167.
[26] E.L. Colla, I.M. Reaney, N. Setter, Effect of structural changes in complex perovskites on the temperature coefficient of the relative permittivity, Journal of Applied Physics 74 (5) (1993) 3414.
[27] M. Onoda, K. Jun, K. Kumiko, et al., $Ba(Zn_{1/3}Nb_{2/3})O_3$–$Sr(Zn_{1/3}Nb_{2/3})$ O_3 solid solution ceramics with temperature-stable high dielectric constant and low microwave loss, Journal of Applied Physics 21 (12) (1982) 1707–1710.
[28] F.S. Galasso, Perovskite and High Tc Superconductors, Gordon and Breach, New York, 1990.
[29] W.I.F. David, Powder diffraction: least-squares and beyond, Journal of Research of National Institute of Standards and Technology 109 (1) (2004) 107–123.
[30] N. Setter, L.E. Cross, The contribution of structural disorder to diffuse phase transitions in ferroelectrics, Journal of Materials Science 15 (10) (1980) 2478–2483.